www.nature.com/npp

American College of Neuropsychopharmacology

ARTICLE

ErbB4 in parvalbumin-positive interneurons mediates proactive interference in olfactory associative reversal learning

Yan Xu[1], Meng-Lin Wang[1], Hui Tao[1,2], Chi Geng[1], Feng Guo[1], Bin Hu[1], Ran Wang[1] and Xiao-Yu Hou[1,2]✉

Consolidated memories influence later learning and cognitive processes when new information is overlapped with previous events. To reveal which cellular and molecular factors are associated with this proactive interference, we challenged mice with odor–reward associative learning followed by a reversal-learning task. The results showed that genetical ablation of ErbB4 in parvalbumin (PV)-positive interneurons improved performance in reversal-learning phase, with no alteration in learning phase, supporting that PV interneuron ErbB4 is required for proactive interference. Mechanistically, olfactory learning promoted PV interneuron excitatory synaptic plasticity and direct binding of ErbB4 with presynaptic Neurexin1β (NRXN1β) and postsynaptic scaffold PSD-95 in the prefrontal cortex. Interrupting ErbB4–NRXN1β interaction impaired network activity-driven excitatory inputs and excitatory synaptic transmission onto PV interneurons. Neuronal activity-induced ErbB4-PSD-95 association facilitated transsynaptic binding of ErbB4–NRXN1β and excitatory synapse formation in ErbB4-positive interneurons. Furthermore, ErbB4–NRXN1β binding was responsible for the activity-regulated activation of ErbB4 and extracellular signal-regulated kinase (ERK) 1/2 in PV interneurons, as well as synaptic plasticity-related expression of brain-derived neurotrophic factor (BDNF). Correlatedly, blocking ErbB4–NRXN1β coupling in the medial prefrontal cortex of adult mice facilitated reversal learning of an olfactory associative task. These findings provide novel insight into the physiological role of PV interneuron ErbB4 signaling in cognitive processes and reveal an associative learning-related transsynaptic NRXN1β-ErbB4-PSD-95 complex that affects the ERK1/2-BDNF pathway and underlies local inhibitory circuit plasticity and proactive interference.

Neuropsychopharmacology (2022) 47:1292–1303; https://doi.org/10.1038/s41386-021-01205-0

INTRODUCTION

Memory consolidation and retrieval are important phases of learning, and thereafter, cognition. Proactive interference affects new learning and hinders the consolidation and retrieval of a new memory if new and established information confuses learners easily, which inhibits cognitive flexibility [1–3]. On the other hand, proactive interference is associated with old memory retention and retrieval, and thus reduces unrelated factors and improves attention in learning. Therefore, elucidating the neural basis for proactive interference is of physiological and pathological significance.

Neural circuitry is dynamically remodeled by learning, which underlies cognitive processes in mammals. Local γ-aminobutyric acid (GABA)ergic inhibitory circuits convert excitatory input signals into inhibitory outputs targeting principal excitatory neurons by feedforward and/or feedback inhibition. Parvalbumin (PV)-positive fast-spiking interneurons account for a majority of inhibitory subpopulations and function as a dominant inhibitory system in the cortex and hippocampus [4, 5]. Multiple lines of evidence indicate that PV interneurons synchronize the firing of principal cells [6, 7] and regulate neural plasticity, learning, and memory [8–14].

In the hippocampus and cortex, PV subtype interneurons highly express ErbB4, which are found to localize at excitatory synapses on PV interneurons [15–20]. Neuregulin 1 (NRG1) is a neurotrophic factor that binds to ErbB proteins [21–23], and NRG1-ErbB4 signaling in the central nervous system has been implicated in neural development, synaptic plasticity, and social memory in adolescence [23–29]. During neurodevelopment, PV interneuron ErbB4 is required for the excitatory synaptogenesis in a cell autonomous manner [15–17, 30]. However, it is unknown if ErbB4 is involved in higher cognitive processes and activity-dependent plasticity of the PV inhibitory circuit in the adult brain.

In this study, we investigate the contributions of PV interneuron ErbB4 to olfactory associative learning and subsequent reversal learning in adult mice. We show that ErbB4 mediates proactive interference in the reversal-learning phase. We also explore the effect of learning-related neuronal activity on excitatory synaptic plasticity of PV interneurons and reveal the underlying molecular basis. Our results uncovered several cellular and molecular mechanisms of ErbB4 signaling behind neural circuit plasticity and cognitive processes.

MATERIALS AND METHODS

Animals

Transgenic *Erbb4*$^{flox/flox}$ (carrying *loxP*-flanked *Erbb4* alleles) mice and PV-Cre mice were kindly from Prof. Lin Mei (Case Western Reserve University). ErbB4 conditional knockout (cKO) mice (PV-*Erbb4*$^{-/-}$) were generated by

[1]Research Center for Biochemistry and Molecular Biology, Jiangsu Key Laboratory of Brain Disease Bioinformation, Xuzhou Medical University, Xuzhou, Jiangsu 221004, China. [2]State Key Laboratory of Natural Medicines, School of Life Science and Technology, China Pharmaceutical University, Nanjing, Jiangsu 211198, China. ✉email: xyhou@cpu.edu.cn

Received: 15 February 2021 Revised: 4 September 2021 Accepted: 2 October 2021
Published online: 27 October 2021

crossing PV-Cre mice with *Erbb4*$^{flox/flox}$ mice as described previously [15, 28]. Rosa26$^{LSL\text{-}tdTomato}$ mice were purchased from Gempharmatech (Nanjing, Jiangsu, China). PV-Cre mice were crossed with Rosa26$^{LSL\text{-}tdTomato}$ mice to generate PV-tdTomato reporter mice. All animals used in this study were housed in a room under a 12 h light/dark cycle with food and water available ad libitum. Experiments were conducted with approval from the local Animal Care and Use Committee according to Regulations for the Administration of Affairs Concerning Experimental Animals (2011) in China.

Antibodies

Mouse monoclonal anti-ErbB4 (MA5-12888) was from Thermo (MA, USA). Rabbit monoclonal anti-ErbB4 (ab32375) was from Abcam (Cambridge, UK). Mouse monoclonal anti-Neurexin1β (MABN607), anti-Myc tag (05-419), anti-CaMKII (05-532), and rabbit polyclonal anti-GST (06-332) were purchased from Millipore (MA, USA). Rabbit polyclonal anti-brain-derived neurotrophic factor (BDNF, sc-546) and mouse monoclonal anti-phospho-ErbB4 (sc-33040) were from Santa Cruz Biotechnology (TX, USA). Rabbit polyclonal anti-p44/42 extracellular signal-regulated kinase 1/2 (ERK1/2, 9102), anti-phospho-p44/42 ERK1/2 (9101), and anti-β-Actin (4970) were obtained from Cell Signaling technology (MA, USA). Guinea pig polyclonal anti-vesicular Glutamate Transporter 1 (vGluT1, AB5905) was from Merck (Darmstadt, Germany). Mouse monoclonal anti-gephyrin (147111) and anti-Neuroligin1 (129111) were from Synaptic System (Goettingen, Germany). Mouse monoclonal anti-PSD-95 (P246) from Sigma (MO, USA) and rabbit polyclonal anti-PV (PV-27) from Swant (London, UK). Horseradish peroxidase (HRP)-conjugated secondary antibodies were from Thermo Pierce (IL, USA). Rabbit polyclonal anti-PSD-95 (51-6900) and Alexa Fluor 488 goat anti-mouse, Alexa Fluor 594 goat anti-guinea pig, and Alexa Fluor 594 goat anti-rabbit secondary antibodies for immunofluorescence were purchased from Invitrogen (MA, USA).

Olfactory associative learning tasks

Mice aged three months, of either sex, were trained in a Go/No-go behavioral task to recognize an odorant using an eight-channel semi-automated olfactometer (Thinker Tech Nanjing Biotech, Nanjing, China). Experiments were conducted in a chamber. An odor port was in the front wall of the chamber, under which was a water delivery spout. Mice were deprived of water two days ago and then learned to lick the water delivery spout (no presentation of odorant) to habituate to the set-up for one day. They were then trained in Go/No-go task. The mouse initiated two-sec-odor delivery in a randomized order by snout insertion in the odor port 0.5 s later. Following a delay of 1.5 s, a reward (10 µl water) was delivered according to odor values when mouse licked the spout. Odor–Reward was paired with a water reward, whereas Odor-No reward received no water. The water value switched on after mice licked in response to Odor–Reward, which was defined as a 'Hit'. During Odor–No reward, mice that did not lick was a correct rejection (CR), whereas mice licked (false alarm, FA) led to 10 s no odor punishment while the mice waited to initiate a new trial. Mice were trained 200 trials each day. The interval between each trial was 4 s. The 200 trials were divided into 10 blocks. Behavioral accuracy was quantified by the percentage of correct trials (percentage of Hit and CR). Odors were diluted to 0.01% in mineral oil to ensure similar vapor pressure. Odors used were isoamyl acetate/2-heptanone (pair 1, Odors A/B) and 2-pentanone/n-amyl alcohol (pair 2, Odors C/D). After pair 2 was completed, we tested the ability of mice to relearn a task if reversed the values attached to the odors of pair 2 (reversal). Mice were water restricted and maintained at 85% of their initial body weight during the training. Data acquisition and analysis were all controlled through computer programs written in LabVIEW (Thinker Tech Nanjing Biotech) and MATLAB (Thinker Tech Nanjing Biotech).

Stereotaxic virus and peptide infusions

ErbB4 cKO mice were anesthetized with isoflurane, and adenovirus recombinants expressing ErbB4-EGFP (Ade-ErbB4-EGFP) and its control Ade-EGFP (OBiO Technology, Shanghai, China) were bilaterally injected to the medial prefrontal cortex (mPFC) using coordinates for the prelimbic cortex: −1.85 mm AP; ±0.5 mm ML; −2.2 mm DV. Virus solution (10^{-7} pfu in 1 µl) was injected at a rate of 0.10 µl/min using a microinfusion pump (RWD Life Science, Shenzhen, China) and sharp glass pipette, and the glass pipette was maintained for 10 min after the injection.

For delivery of interfering peptides, C57BL/6 mice were bilaterally implanted with guide cannulae (RWD Life Science) in the mPFC. After 7 days of recovery, the mice were intracortically infused with a synthetic peptide ErbB4-16P (0.01 nmol, Sangon Biotech, Shanghai, China) or its scrambled control ErbB4-16S (0.01 nmol, Sangon Biotech) under isoflurane inhalation anesthesia. Peptide infusions were at a rate of 0.05 µl/min, and the injection cannula stayed in the guide cannula for 10 min after infusions. An equal volume of 0.9% NaCl served as vehicle control. The mice were subjected to Go/No-go tasks after drug infusion every day. The synthetic peptides were modified by N-terminal acetylation and C-terminal amidation to enhance their stability in vivo.

Primary cortical neuron culture

Primary cortical neurons were prepared as described previously with minor changes [31]. The cortical tissues from embryonic day-18 Sprague–Dawley rats were dissected in ice-cold Dulbecco's modified Eagle medium (DMEM, Gibco, MA, USA) and digested by trypsinization [0.25% (w/v) with 0.02% EDTA, Gibco]. Dissociated neurons were seeded onto poly-D-lysine (Sigma, MO, USA) coated dishes (Φ100 mm) or coverslips (Φ12 mm) at a density of $0.8 \times 10^5/cm^2$ or $0.4 \times 10^5/cm^2$ and cultured in DMEM containing 10% fetal bovine serum (Gibco) and 10% horse serum (Gibco) for 4 h, and the medium were then changed to serum-free Neurobasal medium (Gibco) with 2% B27 (Gibco) and GlutaMAX (0.5 mmol/L, Gibco). After 14 days of culture in vitro (DIV 14), primary cortical neurons were incubated with $GABA_A$ receptor ($GABA_AR$) antagonist bicuculline (Bic, 50 µmol/L, Enzo Life Sciences, NY, USA) for 5 min to induce sustained neuronal activity, or treated with NRG1 (5 nmol/L, R&D Systems, MN, USA) for 30 min. ErbB4-16P (20 µmol/L,) or ErbB4-16S (20 µmol/L, Sangon Biotech) was added 9 h after Bic incubation or 30 min before NRG1 treatment. Tat-tagged ErbB4 C-terminal segment containing amino acids 1288–1308 (Tat-ErbB4CT, Sangon Biotech) or its scrambled control (Tat-scramble, Sangon Biotech) was added for 12 h after Bic treatment.

Label of ErbB4-expressing (ErbB4$^+$) live neurons

ErbB4$^+$ neurons used for electrophysiological experiments were labeled as described previously with slight modifications [32]. Primary cortical neurons (DIV 14) were incubated with anti-extracellular ErbB4 fragment antibody (diluted in Neurobasal medium, final concentration 0.2 µg/µl, Thermo) at 37 °C for 10 min. Neurons were then incubated with Alexa Fluor 488 goat anti-mouse secondary antibody in Neurobasal medium at 37 °C for 10 min and used for whole-cell patch-clamp recording.

Electrophysiology

Excitatory postsynaptic currents (EPSCs) were recorded from the mPFC of PV-tdTomato mice or cultured cortical neurons (DIV 14). PV-tdTomato mice were anesthetized with ketamine/xylazine (140/20 mg/kg, intraperitoneally); then, mice were perfused transcardially with ice-cold artificial cerebral spinal fluid containing (in mmol/L): 124 NaCl, 3 KCl, 1.2 $MgSO_4$, 2.5 $CaCl_2$, 1.23 NaH_2PO_4, 26 $NaHCO_3$, and 10 glucose. Brains were removed quickly, and prefrontal cortical slices (300 µm) were prepared using a Vibroslicer (Leica), incubated with artificial cerebral spinal fluid saturated with 95% O_2 and 5% CO_2 at 28 °C for 1 h prior to whole-cell recording. The EPSCs were recorded using pipettes filled with an internal solution containing (in mmol/L): 10 HEPES, 4 NaCl, 140 K-methylsulfate, 4 MgATP, 0.2 EGTA, 0.3 Na_3GTP, and 10 phosphocreatine at a holding potential of −65 mV. Bic (10 µmol/L) were added to the perfusion solution to block $GABA_AR$-mediated inhibitory postsynaptic currents. For recording the miniature EPSCs (mEPSCs), tetrodotoxin (1 µmol/L) were added to the perfusion solution to block sodium currents. A 5-min recording duration was used for frequency and amplitude analyses. Peak events were detected automatically using an amplitude threshold of twofold the average root mean square noise (15 pA). Mini events were analyzed using MiniAnalysis 6.07 software (Synaptosoft). For recording evoked EPSCs (eEPSCs), monophasic square pulses (200 µs) with gradual increasing intensities (0.15, 0.2, 0.25, and 0.3 mA) were delivered through a concentric electrode that was placed at about 100–150 µm from the recorded neuron located in mPFC layer II/III. Data were filtered at 2 kHz and sampled at 10 kHz. Neurons with a resistance that fluctuated within 15% of initial values were analyzed. The data were amplified using Axopatch-700B and collected using Clampex 10.2 (Molecular Devices, CA, USA).

Protein sample preparation

Brain tissue samples were homogenized in ice-cold homogenization buffer containing 50 mmol/L 3-(N-morpholino) propanesulfonic acid, 320 mmol/L sucrose, 100 mmol/L KCl, 0.5 mmol/L $MgCl_2$, and phosphatase and protease inhibitors (20 mmol/L β-glycerophosphate, 20 mmol/L sodium

pyrophosphate, 50 mmol/L NaF, 1 mmol/L of EGTA, EDTA, sodium orthovanadate, and *p*-nitrophenyl phosphate, 0.5 mmol/L phenylmethylsulfonyl fluoride, 100 μg/ml benzamidine, and 5 μg/ml of aprotinin, leupeptin and pepstatin A). Brain tissue homogenates were centrifuged at 1000 g for 10 min at 4 °C, and the supernatants were collected. Cell samples were lysed in ice-cold homogenization buffer as described above. Protein concentrations were determined using the Lowry method. All samples were stored at −80 °C.

Immunoprecipitation

Protein samples were diluted with immunoprecipitation buffer containing 50 mmol/L HEPES, 150 mmol/L NaCl, 1 mmol/L $ZnCl_2$, 1.5 mmol/L $MgCl_2$, 10% glycerol, 1% Triton X-100, 0.5% Nonidet P-40, and phosphatase and protease inhibitors as indicated above and incubated with primary antibodies overnight at 4 °C, followed by mixing with Protein A Sepharose CL-4B (GE Healthcare Biosciences, Uppsala, Sweden) for 2 h at 4 °C. Immune complexes were isolated by centrifugation. After washing, the bound proteins were subjected to immunoblotting.

Immunoblotting

Samples were boiled for 5 min after addition of 4× sample buffer [0.25 mol/L Tris/HCl (pH 6.8), 8% (w/v) SDS, 20% (v/v) β-mercaptoethanol, 40% (v/v) glycerol, and 0.008% (w/v) bromophenol blue] and separated on sodium dodecyl sulfate-polyacrylamide gels. Protein bands were transferred to nitrocellulose membranes (GE Healthcare Biosciences). After blocking with 3% bovine serum albumin for 3 h, membranes were incubated with the indicated primary antibodies overnight at 4 °C. Antibody binding was detected using HRP-coupled secondary antibody using the Immobilon Western Chemiluminescent HRP Substrate (Millipore). Densitometric analysis was performed using Quantity One 1-D software (Bio-Rad, CA, USA).

HEK293 cell culture and plasmid transfection

HEK293 cells were cultured in DMEM supplemented with 10% fetal bovine serum in dishes (Φ60 mm). Plasmid transfection was performed using polyethyleneimine (Sigma) as described previously [33]. Recombinant plasmids were transfected by incubating 1 μl 10% polyethyleneimine with 2 μg DNA in DMEM and adding to cells at 90% confluence for 2-3 h. After 24 h of transfection, cells were lysed and then analyzed using GST pull-down assays.

The plasmid of Neurexin1β N-terminal fragment (NRXN1βNTF)-Myc was a gift from Prof. Lin Mei (Case Western Reserve University, USA). Recombinant GST-ErbB4 different neighborhood structures 1-331, 332–634, 55-70, 71-86, and 87-100 were generated in pGEX-4T-1. All constructs were verified by DNA sequencing.

GST pull-down assays

Pierce GST Protein Interaction Pull-Down Kit (Pierce Biotechnology, IL, USA) was used to detect the in vitro direct interaction between proteins as described previously [33, 34]. pGEX-4T-1 was used for expressing different truncated ErbB4 regions. GST fusion protein expression was induced in BL21 cells using isopropyl-β-D-thiogalactoside (0.1 mmol/L, Santa Cruz) and immobilized using glutathione agarose. The compound was mixed with 200 μg prey protein sample for 2 h at 4 °C with gentle rocking on a rotating platform. After centrifugation and washing, the bound proteins were eluted and analyzed by immunoblotting.

Immunofluorescence

Mice were anesthetized with isoflurane, and perfused intracardially with 0.9% NaCl and then with 4% formaldehyde. After embedded in low melting point agarose, 50 μm-thick brain slices were cut on a Vibroslicer (Leica). Slices were blocked with 10% normal goat serum in PBS Plus 0.3% Triton-100 (PBST) for 1 h. Primary cortical neurons on coverslips were fixed in 4% formaldehyde for 15 min and incubated with 10% normal goat serum in PBST for 1 h. Brain slices or neurons were incubated with primary antibodies for 24–48 h at 4 °C, washed five times with PBS, and labeled with Alexa Fluor 488 goat anti-mouse, Alexa Fluor 594 goat anti-guinea pig, or Alexa Fluor 594 goat anti-rabbit secondary antibody for 1 h at room temperature. Then nuclei were dyed with 4′,6-diamidino-2-phenylindole (DAPI, Sigma) for 15 min at room temperature. After rinsing five times with PBS, brain slices or neurons were mounted with VECTASHIELD antifade mounting medium (Vector Labs, CA, USA). All antibodies were diluted in PBS containing 10% normal goat serum. Fluorescence images were obtained using a confocal laser-scanning microscope (Zeiss LSM-710, Oberkochen, Germany). Pictures were taken at equal exposure for each group. For quantification of presynaptic boutons, the diameter was set between 0.6 and 1.1 μm for vGluT1 as reported size ranges previously [35]. For immunostaining of postsynaptic puncta in PV or CaMKII-positive neurons, region of interest (ROI) was selected from random dendrite within 20 μm of the proximal cell body. The total levels of pERK1/2 were determined by tracing the outline of the cell body and the dendrite branches of neurons.

Quantification and statistical information

Statistical analysis was performed using GraphPad Prism 7.0. Go/No-Go behavioral task, immunostaining, and electrophysiological results are presented as means ± standard errors of measurement. Immunoblotting results are presented as mean ± standard deviation of data from at least three independent experiments. Differences between groups were assessed using *t*-tests or analysis of variance (ANOVA), which were indicated in the figure legends. $P < 0.05$ was considered statistical significance.

RESULTS

ErbB4 conditional knockout in PV interneurons facilitates olfactory associative reversal learning in adult mice

To investigate whether PV neuron ErbB4 is involved in olfactory associative learning, and thereafter reversal learning, we generated PV-specific ErbB4 cKO mice (PV-*Erbb4*$^{-/-}$) by crossing the *Erbb4*-floxed mice with the PV-Cre mice (PV-*Erbb4*$^{+/+}$). The PV-*Erbb4*$^{-/-}$ mice and their littermate controls (PV-*Erbb4*$^{+/+}$) were challenged with an odor–reward associative (Go/No-go) task to learn to make a discrimination, followed by a reversal-learning task to reverse their choice. As shown in Fig. 1A, mice were trained with two odor pairs (Odors A/B: isoamyl acetate/2-heptanone, Odors C/D: 2-pentanone/n-amyl alcohol); each odor was associated with the choice of water licking (Odor–Reward: Go) or not licking (Odor-No reward: No-go). Hit and CR were the correct responses to different odor value, while Miss and FA were the incorrect ones. The percentage Hit and/or CR accuracy were used to evaluate the performance of mice in Go/No-go learning (Fig. 1B and C).

On Day 1, mice learned to discriminate Odor A (Reward) from Odor B (No-reward) with an accuracy of about 80% after 10 blocks (200 trials) (Fig. 1B). During the next 10 blocks on Day 2, the accuracy remained above 80% (Fig. 1B). On Day 3, the discrimination of another pair (Odors C/D) was readily accomplished with an accuracy of 80% (Fig. 1B). The learning curve of PV- *Erbb4*$^{-/-}$ mice was not significantly different from that of PV-*Erbb4*$^{+/+}$ mice through Day 1 to Days 3, indicating that the ablation of ErbB4 in PV neurons does not affect new associative learning, memory consolidation, and retrieval, or the sense of smell. Interestingly, when the associations of Odors C and D were interchanged on Day 4 and Day 5, PV-*Erbb4*$^{+/+}$ mice needed many more blocks of training to reach an accuracy of 80%; in contrast, PV-*Erbb4*$^{-/-}$ mice exhibited better performance (Fig. 1B), while the recovery of ErbB4 expression by Ade-ErbB4-EGFP infusion abolished the performance improvement in the reversal learning phase (Fig. S1A). Moreover, we found that the performance of PV-*Erbb4*$^{-/-}$ mice with regard to CR, but not Hit, was better than that of PV-*Erbb4*$^{+/+}$ mice (Fig. 1C) and Ade-ErbB4-EGFP infusion mice (Fig. S1B), indicating that reward facilitates associative learning and memory, previous reward-associative information interferes with new learning, and PV neuron cKO of ErbB4 weakens this interference.

Taken together, the above data suggest that ErbB4 in PV-expressing interneurons contributes to proactive interference in the reversal phase of olfactory associative learning. PV neuron ErbB4 is required for the stability or retrieval of a memory and thus it takes more trials to weaken the interference of old conflicting information.

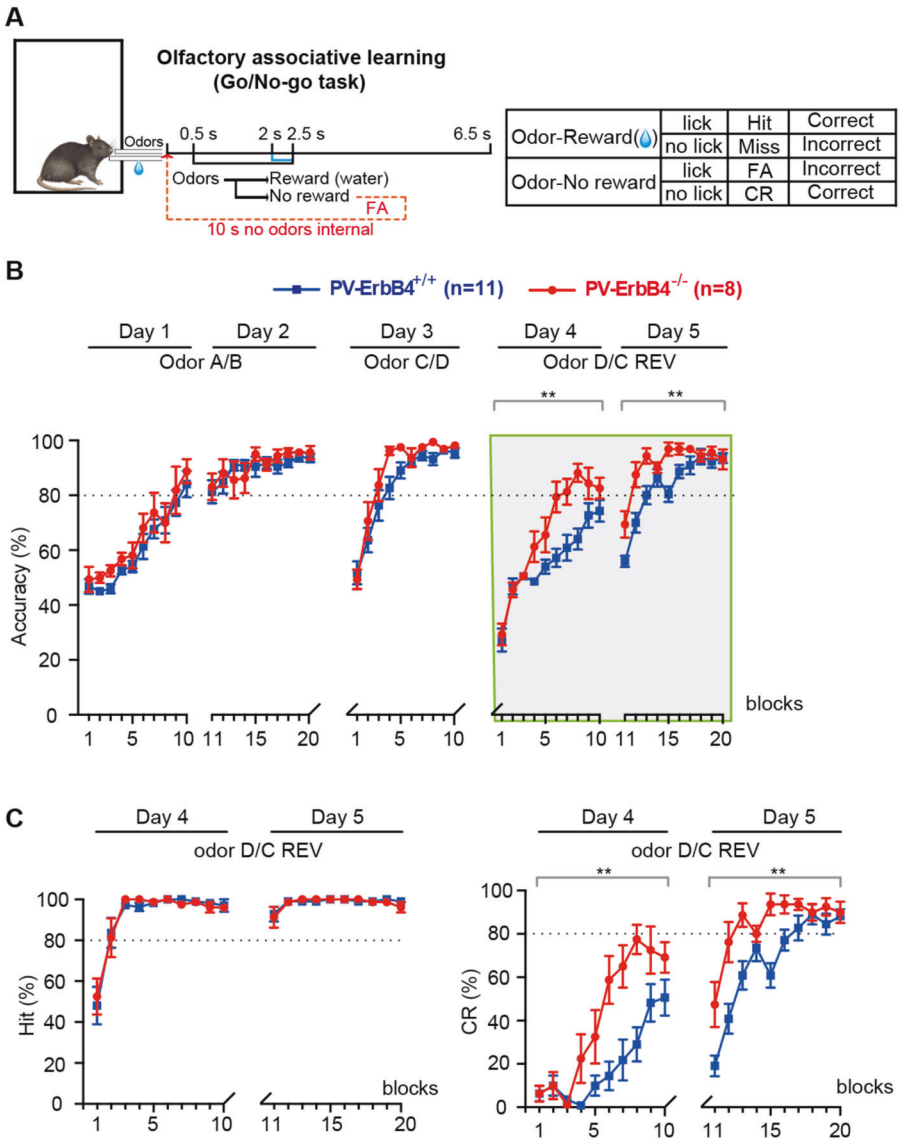

Fig. 1 ErbB4 conditional knockout in PV interneurons facilitates olfactory associative reversal learning in adult mice. A Behavioral paradigm of olfactory associative learning with Go/No-go tasks. The schematic describes the time course of a single trial. Mice insert their snouts into odor port to trigger Odors. Mice lick under Odor–Reward is paired with a water reward (Hit). In response to Odor-No reward, no lick is a correct rejection (CR), whereas lick (false alarm, FA) will lead to 10 s of no odor punishment. **B** Mice learned to discriminate the value of the two pair odors (Odors A/B: isoamyl acetate *versus* 2-heptanone, Odors C/D: 2-pentanone *versus* n-amyl alcohol) with water reward for the first three days, and then the value of Odors C/D was reversed (Odor D/C REV) in the next two days (Day 4 and 5). Accuracy shown during Go/No-go tasks was the percentage of correct choices (Hit and CR) for odor pairs. Data shown are mean ± SEM. $^{**}P < 0.01$. $F(1, 17) = 12.21$, $P = 0.0028$ in Day 4; $F(1, 17) = 8.612$, $P = 0.0093$ in Day 5, two-way repeated-measures ANOVA. **C** The accuracy with regard to Hit or CR in the reversal phase. Data shown are mean ± SEM. $^{**}P < 0.01$. $F(1, 17) = 8.887$, $P = 0.0084$ in Day 4 of CR; $F(1, 17) = 10.35$, $P = 0.0051$ in Day 5 of CR, two-way repeated-measures ANOVA.

Learning-related neuronal activity promotes PV neuron excitatory synaptic plasticity and induces the interaction of ErbB4 with NRXN1β and PSD-95 in cortical neurons

The PFC is critical for reinforcement learning and mediates learning flexibility [36]. During learning consolidation, the PFC is responsible for memory acquisition, which fundamentally depends on the hippocampus [37]. Since reversal learning is weakened by previous memory and ErbB4 is related to the interference, we next investigated the role of ErbB4 in the PFC in previous memory. After PV-tdTomato mice have learned to discriminate Odor C (Reward) from Odor D (No reward) over 400 trials in 2 days, immunofluorescence assay showed that the density of vGluT1^{+} glutamatergic presynaptic terminals (vGluT1 buttons) onto PV interneurons increased in the mPFC (Fig. 2A). Furthermore, excitatory synaptic transmission of PV interneurons in the mPFC were measured in whole-cell patch-clamping mode. As shown in Fig. 2B, the amplitude and frequency of mEPSCs in mPFC PV interneurons increased after Go/No-go task training. Strikingly, there was an upward shift of input–output (I/O) curves of eEPSCs in trained mice compared with those in the untrained group (Fig. 2C). These results suggest that olfactory learning enhances excitatory synaptic plasticity of PV neurons in the PFC.

Neurexins (NRXNs) are a family of presynaptic adhesion proteins that help to connect neurons at the synapses [38–40]. Each neurexin(1–3) gene has two promoters that drive the synthesis of the longer NRXN(1-3)α and shorter NRXN(1-3)β proteins. NRXNβs play essential roles in the regulation of excitatory synaptic circuits

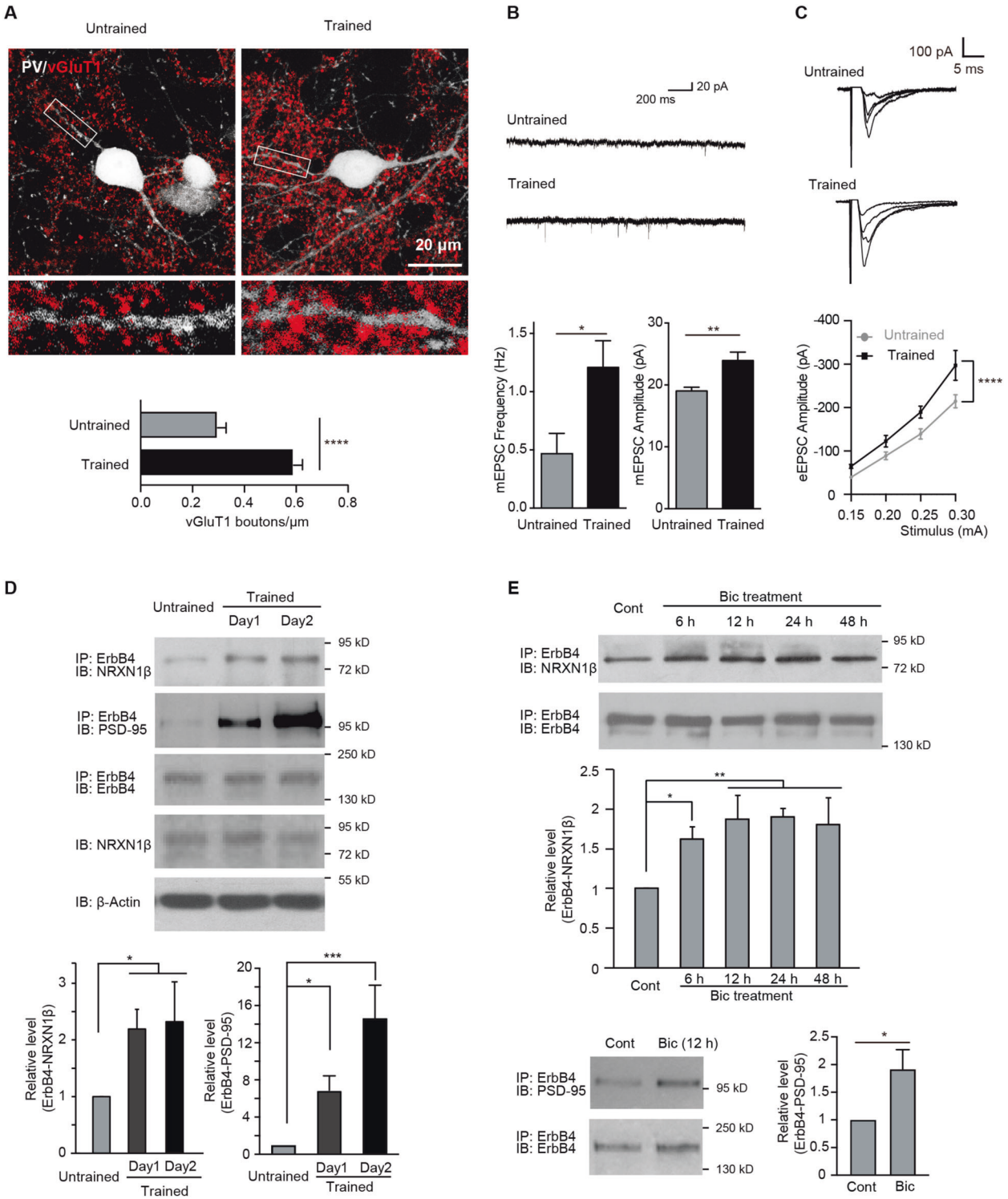

and contextual fear memory [38]. Of the three NRXNβ proteins, NRXN1β predominantly localizes at excitatory axon terminals of pyramidal neurons [39]. To test molecular events behind the enhancement of excitatory synaptic plasticity in PV neurons, we examined the interactions of ErbB4 with excitatory presynaptic adhesion molecule NRXN1β and postsynaptic scaffolding protein PSD-95. Co-immunoprecipitation (Co-IP) analysis showed that olfactory associative learning promoted ErbB4 interaction with NRXN1β and PSD-95 in the PFC (Fig. 2D), but not in the hippocampus (Fig. S2), implicating the involvement of NRXN1β-ErbB4-PSD-95 complex in learning-induced excitatory synaptic plasticity of PV interneurons.

PV-expressing interneurons have been believed to be critical cellular substrates of cognitive processes [10, 41]. To elucidate how PV interneurons sense corresponding network activity, we investigated the interactions of ErbB4–NRXN1β and ErbB4–PSD-95 following neuronal activity upregulation in primary cortical neurons. Cortical cultures were exposed to the $GABA_AR$ antagonist Bic for 5 min to restrain tonic GABAergic inhibition and trigger N-methyl-D-aspartate receptor (NMDAR)-dependent sustained

Fig. 2 Olfactory learning and neuronal activity upregulate PV neuron excitatory synaptic plasticity and induce the interactions of ErbB4 with NRXN1β and PSD-95. A Brain slices were immunostained using anti-vGluT1 antibody. Confocal image showing vGluT1 boutons apposed to the PV interneurons. Scale bar = 20 μm. Histogram shows mean ± SEM ($n = 14$ cells from three untrained mice or 15 cells from three trained mice). ****$P < 0.0001$, unpaired t-tests. **B–C** PV interneuron miniature excitatory postsynaptic currents (mEPSCs) or evoked excitatory postsynaptic currents (eEPSCs) were recorded in the medial prefrontal cortex region. Representative traces in PV interneurons are from untrained or trained PV-tdTomato mice. Data are presented as mean ± SEM ($n = 11$ cells from three untrained mice or 11 cells from three trained mice). *$P < 0.05$, **$P < 0.01$, ****$P < 0.0001$. $t = 2.573$, df = 20, $P = 0.0182$ for mEPSC Frequency; $t = 3.233$, df = 20, $P = 0.0042$ for mEPSC Amplitude; unpaired t-tests. F (1, 84) = 17.16, $P < 0.0001$ for eEPSC Amplitude, two-way ANOVA. **D** Mice were trained in the Go/No-go task for one or two days. Interaction between ErbB4 and NRXN1β or PSD-95 in the prefrontal cortex of mice was measured using Co-immunoprecipitation (Co-IP) with an anti-ErbB4 antibody followed by immunoblotting (IB) with an anti-NRXN1β or PSD-95 antibody. Results are normalized to those of their respective untrained groups. Data are presented as mean ± SD ($n = 3$). *$P < 0.05$, ***$P < 0.001$ (compare each group with Untrained group). For ErbB4–NRXN1β interaction: F(2, 6) = 7.81, $P = 0.0314$ (Day 1); $P = 0.0205$ (Day 2). For ErbB4-PSD-95 interaction: F(2, 6) = 0.8399, $P = 0.0327$ (Day 1), $P = 0.0006$ (Day 2); one-way ANOVA with Dunnett's method. **E** Primary cultured cortical neurons were incubated with bicuculline (Bic, 50 μmol/L) and analyzed for the indicated time after Bic treatment. Results are normalized to those of their respective controls (Cont) and expressed as mean ± SD ($n = 3$). *$P < 0.05$, **$P < 0.01$ (compare each group with Cont group). For ErbB4–NRXN1β interaction: F(4,10) = 8.77, $P = 0.0203$ (Bic 6 h); $P = 0.0023$ (Bic 12 h); $P = 0.0017$ (Bic 24 h); $P = 0.0036$ (Bic 48 h). One-way ANOVA with Dunnett's method. For ErbB4-PSD-95 interaction: $t = 4.506$, df = 2, $P = 0.0459$, t tests.

synaptic activity [33]. As shown in Fig. 2E, Bic treatment-triggered activity induced significant increases in both ErbB4–NRXN1β and ErbB4–PSD-95 interactions. Neuroligin1 (NL1) functions as a postsynaptic ligand of NRXN1β [42]. However, unlike the long-lasting interaction of ErbB4–NRXN1β, persistent network activation only mediated transient binding of NL1 with NRXN1β (Fig. S3). These findings suggest that the NRXN1β-ErbB4-PSD-95 complex is dynamically regulated by neuronal network activity.

The extracellular N-terminus of ErbB4 binds NRXN1β directly

The ErbB4 N-terminal fragment (NTF, amino acids 1-634) consists of two cysteine-rich domains (CRDs) flanking a putative receptor L domain (Fig. 3A). GST pull-down analysis showed that the NRXN1βNTF directly bound ErbB4 fragments representing amino acids 1–331 but did not bind with fragments representing amino acids 332–634 (Fig. 3B). Furthermore, we confirmed a strong affinity between NRXN1βNTF and ErbB4 NTF representing amino acids 71-86, while weak affinity between NRXN1βNTF and amino acids 87-100 of ErbB4 (Fig. 3C). These results prove that the N-terminus of ErbB4 corresponding to amino acids 71-100, especially amino acids 71–86 (a region herein referred to as ErbB4 71–86), directly binds to NRXN1β extracellular domains.

A small peptide ErbB4-16P, with an amino acid sequence homologous to that of ErbB4 71–86, and random scrambled control (ErbB4-16S) were synthesized. Using GST pull-down studies, we found that ErbB4-16P, but not ErbB4-16S, competitively blocked ErbB4–NRXN1β binding (Fig. 3D) in a dose-dependent manner. This result further demonstrates the direct binding between the N-terminus of ErbB4 and the extracellular domains of NRXN1β. Moreover, in cultured primary cortical neurons, incubation with ErbB4-16P reduced the level of ErbB4–NRXN1β binding induced by Bic-evoked neuronal activity (Fig. 3E). NRG1 incubation induced the activation (tyrosine phosphorylation) of ErbB4 in cultured cortical neurons. Pretreatment of ErbB4-16P showed no effect on ErbB4 tyrosine phosphorylation in response to NRG1 (Fig. S4), suggesting that ErbB4-16P does not affect NRG1-ErbB4 signaling.

ErbB4–NRXN1β interaction mediates the activity-mediated excitatory inputs onto PV interneurons and activates plasticity-related signaling

Considering the in vivo excitatory postsynaptic distribution of ErbB4 in PV neurons, and presynaptic distribution of NRXN1β in axonal segments of excitatory pyramidal rather than PV neurons, we hypothesized that ErbB4 association with NRXN1β facilitates excitatory synapse formation in PV interneurons. Cortical cultures were exposed to Bic for 5 min to induce neuronal activity. Immunofluorescence assay showed that in PV interneurons, the number and size of PSD-95 (a postsynaptic marker of excitatory synapses) puncta increased after Bic treatment, while ErbB4-16P decreased the number and size of PSD-95 puncta (Fig. 4A). No difference was observed in gephyrin (a postsynaptic marker of inhibitory synapses) puncta among groups (Fig. S5A). On the other hand, in CaMKII-positive glutamatergic neurons, inhibiting the ErbB4–NRXN1β interaction did not alter the number and size of PSD-95 puncta (Fig. S5B). The data suggest that ErbB4–NRXN1β binding is required for neuronal activity-induced excitatory afferents onto PV interneurons.

PSD-95 directly binds ErbB4 C-terminal motif, which causes ErbB4 translocation into lipid rafts in the postsynaptic density [20, 43]. We wondered whether the activity-induced ErbB4-PSD-95 binding is linked to the ErbB4–NRXN1β combination. As shown in Fig. S6A and S6B, co-immunoprecipitation results showed that neuronal activity promoted the ErbB4-PSD-95 association in primary cortical neurons; Tat-ErbB4CT, but not Tat-scramble, disrupted not only the ErbB4-PSD-95 binging but also the ErbB4–NRXN1β binding. Furthermore, immunofluorescence analysis showed that Tat-ErbB4CT inhibited activity-induced excitatory afferents onto ErbB4$^+$ neurons (Fig. S6C). The above findings provide evidence that PSD-95 recruits ErbB4 into excitatory synapses, which augments transsynaptic ErbB4–NRXN1β signaling following sustained neuronal activity.

BDNF, a member of the neurotrophin family of growth factors, is believed to modulate the number and structure of excitatory synapses [33, 44]. As shown in Fig. 4B, the expression levels of BDNF were upregulated following neuronal activity enhancement by Bic, and ErbB4-16P reduced BDNF levels in cortical neurons. To further investigate the mechanisms underlying activity-induced excitatory synapse formation and maturation on PV interneurons, we examined the contribution of transsynaptic ErbB4–NRXN1β binding to the activation of ErbB4-ERK1/2 signaling. The phosphorylation levels of ErbB4 and ERK1/2 increased after Bic treatment. Co-treatment with ErbB4-16P, but not ErbB4-16S, attenuated both ErbB4 and ERK1/2 activation (Fig. 4B). Using the immunofluorescence method, we further confirmed that ErbB4-16P specifically inhibited the phosphorylation level of ERK1/2 in ErbB4$^+$ neurons but not pyramidal neurons (Fig. 4C). These findings suggest a critical role of NRXN1β-ErbB4-ERK1/2 signal events in activity-evoked excitatory synaptic plasticity in PV interneurons.

Blocking ErbB4–NRXN1β interaction impairs excitatory synaptic responses of ErbB4-expressing interneurons and improves olfactory associative reversal learning

Furthermore, we investigated the effect of ErbB4-16P on excitatory synaptic responses in cultured cortical neurons. ErbB4$^+$ neurons were live-labeled using an antibody against the extracellular N-terminus of ErbB4. Whole-cell patch-clamp recording

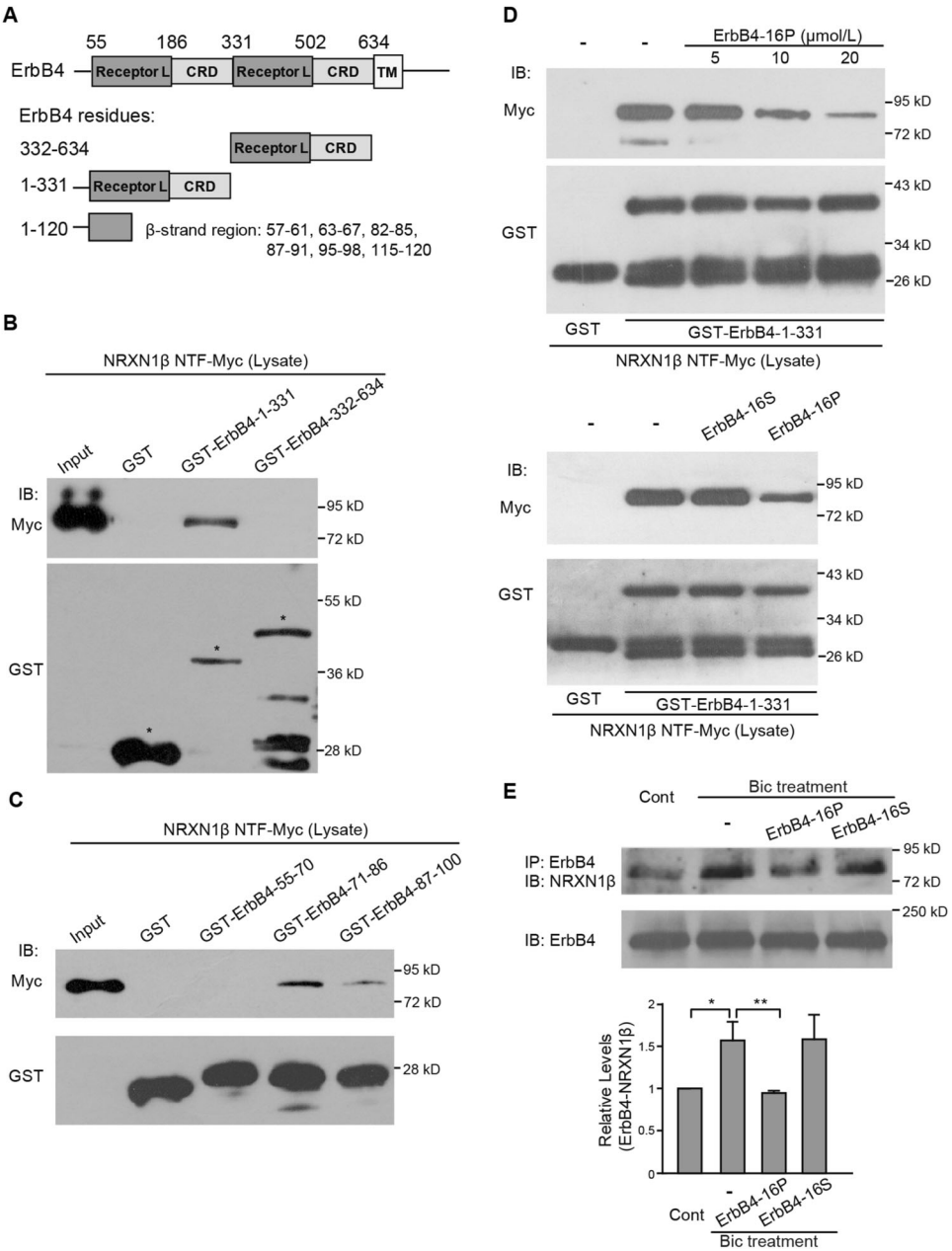

Fig. 3 The extracellular N-terminus of ErbB4 binds NRXN1β directly. A Schematic diagram describing the extracellular domain of ErbB4. TM refers to the transmembrane domain. The extracellular domain of ErbB4 primarily contains receptor L and cysteine-rich domains (CRDs). **B**, **C** Direct binding between ErbB4 and NRXN1β was analyzed using GST pull-down. A series of GST-ErbB4 truncated fusion proteins were expressed in BL21 cells and then collected. HEK293 cells were transfected with NRXN1βNTF-Myc and then NRXN1βNTF-Myc in the cell lysate was pulled down by a GST-fused ErbB4 segment representing AAs 1-331, mainly pulled down by GST-tagged AAs 71-86 of ErbB4. Asterisk refers to GST or GST-fused protein. **D** ErbB4-16P specifically inhibited ErbB4–NRXN1β interaction in a dose-dependent manner. NRXN1βNTF-Myc in the HEK293 cell lysate was incubated with ErbB4-16P (5, 10, 20 μmol/L) or ErbB4-16S (20 μmol/L) for 40 min and then pulled down using GST-fused ErbB4 1-331. The results are representative of three independent experiments. **E** Primary cortical neurons were post-incubated with ErbB4-16P (20 μmol/L) or ErbB4-16S (20 μmol/L) 9 h after bicuculline (Bic) treatment. Co-immunoprecipitation (Co-IP) followed by immunoblotting (IB) was used to detect NRXN1β-ErbB4 binding. Results were normalized to control (Cont) groups and expressed as mean ± SD ($n = 3$). $^{*}P < 0.05$, $^{**}P < 0.01$ (compare each group with Bic group). $F(3, 8) = 10.12$, $P = 0.0164$ (Cont); $P = 0.0098$ (Bic + ErbB4-16P); $P = 0.9992$ (Bic + ErbB4-16S). One-way ANOVA with Dunnett's method.

showed that both frequency and amplitude of mEPSCs increased after Bic treatment, and ErbB4-16P inhibited such increase in frequency and amplitude in ErbB4-positive neurons (Fig. 5A). These results suggest that ErbB4–NRXN1β interaction facilitates excitatory synaptic transmission onto ErbB4-positive interneurons.

To determine whether ErbB4–NRXN1β interaction in the mPFC is required for associative reversal learning, we adopted ErbB4-16P to block the ErbB4–NRXN1β coupling during Go/No-go task and subsequent reversal learning phase. After the mice were habituated to the experimental chamber, ErbB-16P, ErbB4-16S, or vehicle control was daily infused into the mPFC of mice through the implanted microcannula for six consecutive days. We found that the learning curve in mice treated with ErbB4-16P or ErbB4-16S was not significantly different from that of vehicle-treated mice through Day 1–Day 3 (Fig. 5B). However, when the associated values of Odors C and D were interchanged on Day 4, mice treated with ErbB4-16P

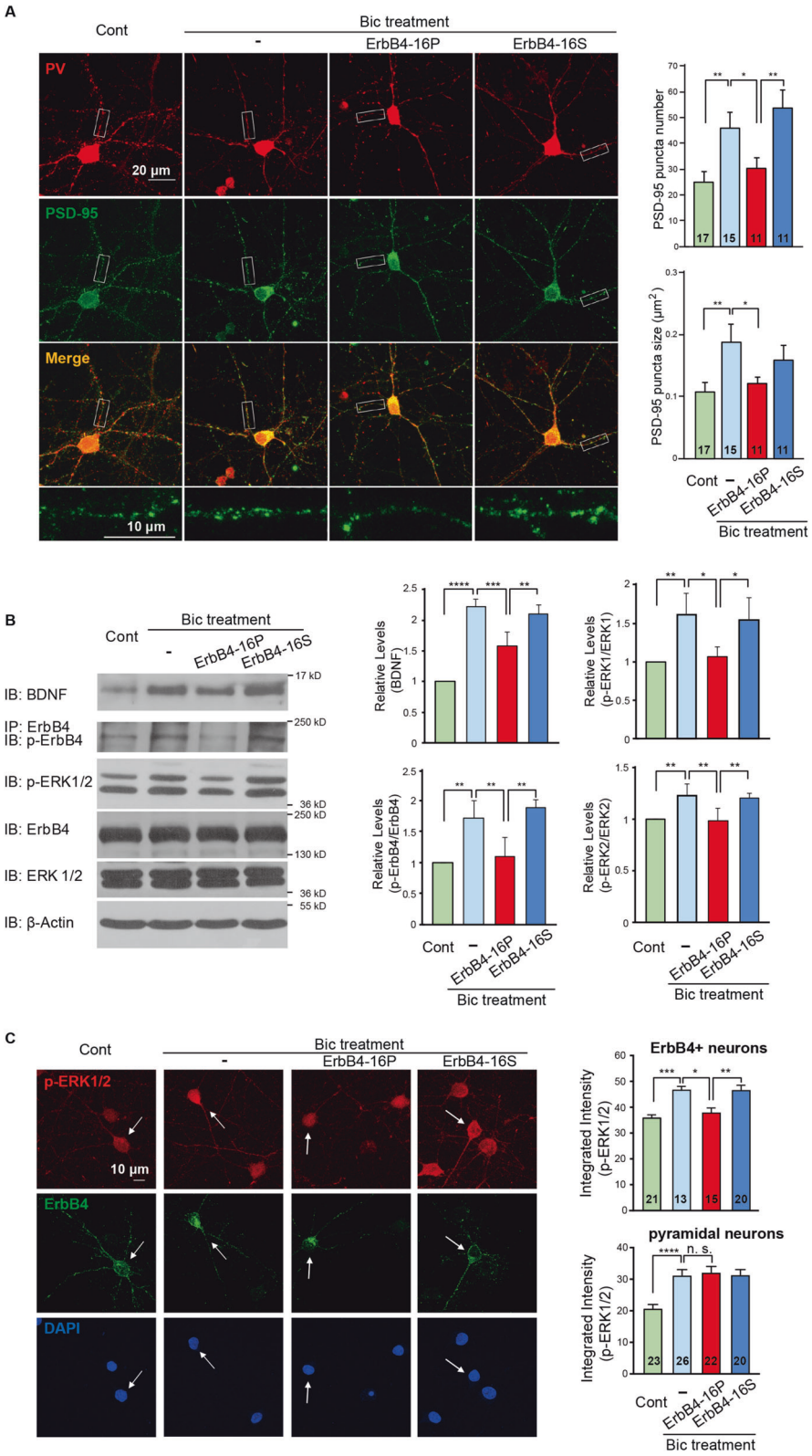

displayed significantly enhanced accuracy compared with vehicle group (Fig. 5B). As shown in Fig. 5C, the performance of ErbB4-16P-treated mice with regard to CR, but not Hit, was better than that of vehicle-treated mice on the first day of reversal-learning tasks (Day 4). In addition, when ErbB4-16P or ErbB4-16S was administered during the reversal task (Day 4–Day 6), ErbB4-16P still slightly enhanced reversal learning compared with ErbB4-16S (Fig. S7A, not significant, $P = 0.0724$), especially improved the performance with regard to CR on Day 4 (Fig. S7B, $P < 0.01$). These data indicate that ErbB4–NRXN1β interaction facilitates the stability or retrieval of reward-related old memory, which will interfere with similar new learning.

Fig. 4 Blocking ErbB4–NRXN1β interaction interrupts the activity-mediated excitatory inputs onto PV interneurons and attenuates ERK1/2-BDNF signaling. A Primary cortical neurons were post-incubated with ErbB4-16P (20 μmol/L) or ErbB4-16S (20 μmol/L) 9 h after bicuculline (Bic) treatment and immunostained 24 h after Bic treatment. PV and PSD-95 were co-stained to represent excitatory synapses on PV interneurons. The boxed area (a 20 μm segment) was enlarged in the respective bottom image and puncta (number and size) were measured from five independent experiments. Histograms show mean ± SEM ($n = 17$, 15, 11, and 11 cells for each group). *$P < 0.05$, **$P < 0.01$, (n.s. refers to non-significance). $F(3,50) = 7.454$, Bic vs controls (Cont), Bic + ErbB4-16P, Bic + ErbB4-16S: $P = 0.0014$, $P = 0.0242$, $P = 0.3458$, respectively; Bic + ErbB4-16P vs Bic + ErbB4-16S, $P = 0.0037$ for PSD-95 puncta number. $F(3,50) = 4.764$, Bic vs Cont, Bic + ErbB4-16P, Bic + ErbB4-16S: $P = 0.0010$, $P = 0.0119$, $P = 0.2657$, respectively; Bic + ErbB4-16P vs Bic + ErbB4-16S, $P = 0.1725$ for PSD-95 puncta size. One-way ANOVA with Tukey's method. **B**, **C** Primary cortical neurons were post-incubated with ErbB4-16P (20 μmol/L) or ErbB4-16S (20 μmol/L) 9 h after Bic treatment and performed experiments 12 h after Bic treatment. In (**B**), cell lysates were subjected to the co-immunoprecipitation (Co-IP) or immunoblotting (IB) using the indicated antibodies. Results are normalized to Cont groups and expressed as mean ± SD ($n = 3$). *$P < 0.05$, **$P < 0.01$, ***$P < 0.001$, ****$P < 0.0001$. $F(3,8) = 44.69$, Bic vs Cont, Bic + ErbB4-16P, Bic + ErbB4-16S: $P < 0.0001$, $P = 0.0007$, $P = 0.3825$, respectively; Bic + ErbB4-16P vs Bic + ErbB4-16S, $P = 0.0023$ for relative levels of BDNF. $F(3,8) = 13.01$, Bic vs Cont, Bic + ErbB4-16P, Bic + ErbB4-16S: $P = 0.0031$, $P = 0.0072$, $P = 0.3703$, respectively; Bic + ErbB4-16P vs Bic + ErbB4-16S, $P = 0.0019$ for relative levels of p-ErbB4/ErbB4. $F(3,8) = 6.705$, Bic vs Cont, Bic + ErbB4-16P, Bic + ErbB4-16S: $P = 0.0077$, $P = 0.0137$, $P = 0.7141$, respectively; Bic + ErbB4-16P vs Bic + ErbB4-16S, $P = 0.0245$ for relative levels of p-ERK1/ERK1. $F(3,8) = 0.0026$, Bic vs Cont, Bic + ErbB4-16P, Bic + ErbB4-16S: $P = 0.0021$, $P = 0.0015$, $P = 0.4264$, respectively; Bic + ErbB4-16P vs Bic + ErbB4-16S, $P = 0.0048$ for relative levels of p-ERK2/ERK2. One-way ANOVA with Tukey's method. In (**C**), primary cortical neurons were immunostained with anti-p-ERK1/2 and anti-ErbB4 antibodies. DAPI was used to stain the neuron nuclei. The arrows directed to $ErbB4^+$ neurons. Histograms show mean ± SEM (from three independent experiments, $n = 21$, 13, 15, and 20 cells for each group in $ErbB4^+$ neurons, $n = 23$, 26, 22, and 20 cells in pyramidal neurons). *$P < 0.05$, **$P < 0.01$, ***$P < 0.001$, ****$P < 0.0001$ (n.s. refers to non-significance). $F(3, 65) = 10.53$, Bic vs Cont, Bic + ErbB4-16P, Bic + ErbB4-16S: $P = 0.0006$, $P = 0.0120$, $P = 0.9999$, respectively; Bic + ErbB4-16P vs Bic + ErbB4-16S, $P = 0.0053$; top panel. $F(3, 87) = 10.57$, Bic vs Cont, Bic + ErbB4-16P, Bic + ErbB4-16S: $P < 0.0001$, $P = 0.9874$, $P > 0.9999$, respectively; Bic + ErbB4-16P vs Bic + ErbB4-16S, $P = 0.9888$; bottom panel. One-way ANOVA with Tukey's method.

DISCUSSION

ErbB4 is mainly expressed in PV interneurons and regulates GABA release, neurodevelopment, and synapse plasticity in the PFC and hippocampus [15–20, 26, 45]. In that context, we found that ErbB4 in PV interneurons hinders olfactory associative learning in the reversal phase. We also found that associative learning facilitates the associations of ErbB4 in PV interneurons with excitatory presynaptic NRXN1β and postsynaptic PSD-95, which mediates excitatory inputs onto PV neurons and accounts for the contribution of ErbB4 to proactive interference in reversal learning. Our results identify the role of ErbB4 proteins as transsynaptic organizers responsible for the excitatory synaptic plasticity of PV interneurons and higher cognitive processes.

Proactive interference comes from previous experience, which impedes the encoding of new conflicting information [46]. However, the cellular and molecular mechanisms underlying proactive interference are unclear. In this study, we showed that ErbB4 in PV neurons does not affect olfactory associative learning, memory consolidation, and associative information retrieval, but reduces the performance of mice in learning and remembering a new, conflicting (but not non-conflicting) association. It means that ErbB4 in PV neurons is beneficial for the accumulation of experience and rapid/appropriate responses to similar situations next time, although it seems to make a learner inflexible. It is easily understood that a reward makes learning more effective and memory retained longer, and thus disturbs new learning [47]. We also provided evidence that an original reward enhances the encoding of an associative event via the PV interneuron ErbB4 pathway, which displays proactive interference in reversal learning. At the same time, a reward promotes the encoding of conflicting association, which abolishes the ErbB4-mediated proactive interference. Thus, reward associative training is a better way for overcoming proactive interference.

The PFC is an integral part of the neural network and is crucial for memory consolidation, retrieval, and extinction [48]. We found that ErbB4 is required for PV interneurons to sense olfactory learning-evoked network activity by transsynaptically binding to excitatory presynaptic NRXN1β in the PFC region, but not in the hippocampus of mice. NMDAR-dependent persistent neuronal activity facilitates ErbB4–NRXN1β binding in primary cortical neurons. These findings suggest that the ErbB4–NRXN1β interaction is neuronal activity-dependent, hinting that olfactory associative learning does not induce long-lasting network activity in the olfacto-hippocampal circuitry, but depends on the olfacto-PFC circuitry. Learning-induced excitatory transmission onto PV neurons upregulates GABA release and downregulates local network activity in the PFC. Recent findings with muscimol (a $GABA_AR$ agonist) supported that mPFC inactivation is involved in proactive interference [49, 50].

Neural circuitry remodeling underlies perceptual and cognitive processes in the brain [51, 52]. Synaptic adhesion proteins are responsible for synapse formation [53–55]; acting as presynaptic cell-adhesion molecules, NRXNs are known to regulate synapse properties via integrating multiple postsynaptic binding partners, including neuroligin, leucine-rich repeat transmembrane neuronal proteins, dystroglycan, etc. [41, 56, 57], transmit different transsynaptic signals, and shape the input/output relations of local neural circuits [58]. Thus, NRXNs and their ligands present dynamic combinations regulated by network activity [59, 60]. Here, we found that NMDAR-dependent neural network activation only transiently induces the binding of NL1 with NRXN1β. We first report that, unlike the transient NRXN1β-NL1 interaction, ErbB4 and NRXN1β form permanent transsynaptic bridges. These findings suggest that the ErbB4–NRXN1β signal is more valuable in learning-induced persistent neuronal circuitry remodeling.

The extracellular region of ErbB4 consists of two CRDs flanking two receptor L repeats. The ErbB4 NTF (amino acids 71-86) is the major NRXN1β-binding motif. Our study reveals that neuronal activity-induced NRXN1β-ErbB4 binding promotes synaptic transmission onto PV interneurons. Moreover, the NRXN1β-ErbB4 binding stimulates ERK1/2 activity and BDNF expression. In the adult brain, BDNF expression and release play important roles in synapse formation and synaptic plasticity [33, 44, 61]. We now show that neuronal activity induces ErbB4 activation through transsynaptic binding of NRXN1β and promotes BDNF expression which is abolished by interruption of NRXN1β-ErbB4 binding. BDNF expression and release are controlled by neuronal activity, which has been found to be damaged in patients with depression [62]. The deficits in GABAergic transmission induce depressive-like behavioral and cognitive dysfunction [63]. It would be interesting to further investigate the presynaptic and postsynaptic mechanisms behind NRXN1β-ErbB4-mediated ERK1/2-BDNF signaling, the alteration of NRXN1β-ErbB4-BDNF signaling in depression models, and its contributions to depressive-like behavioral and cognitive dysfunction.

Severe deficits in overcoming proactive interference have been found in aging and neuropsychiatric disorders including depression and post-traumatic stress disorder (PTSD) [64–66].

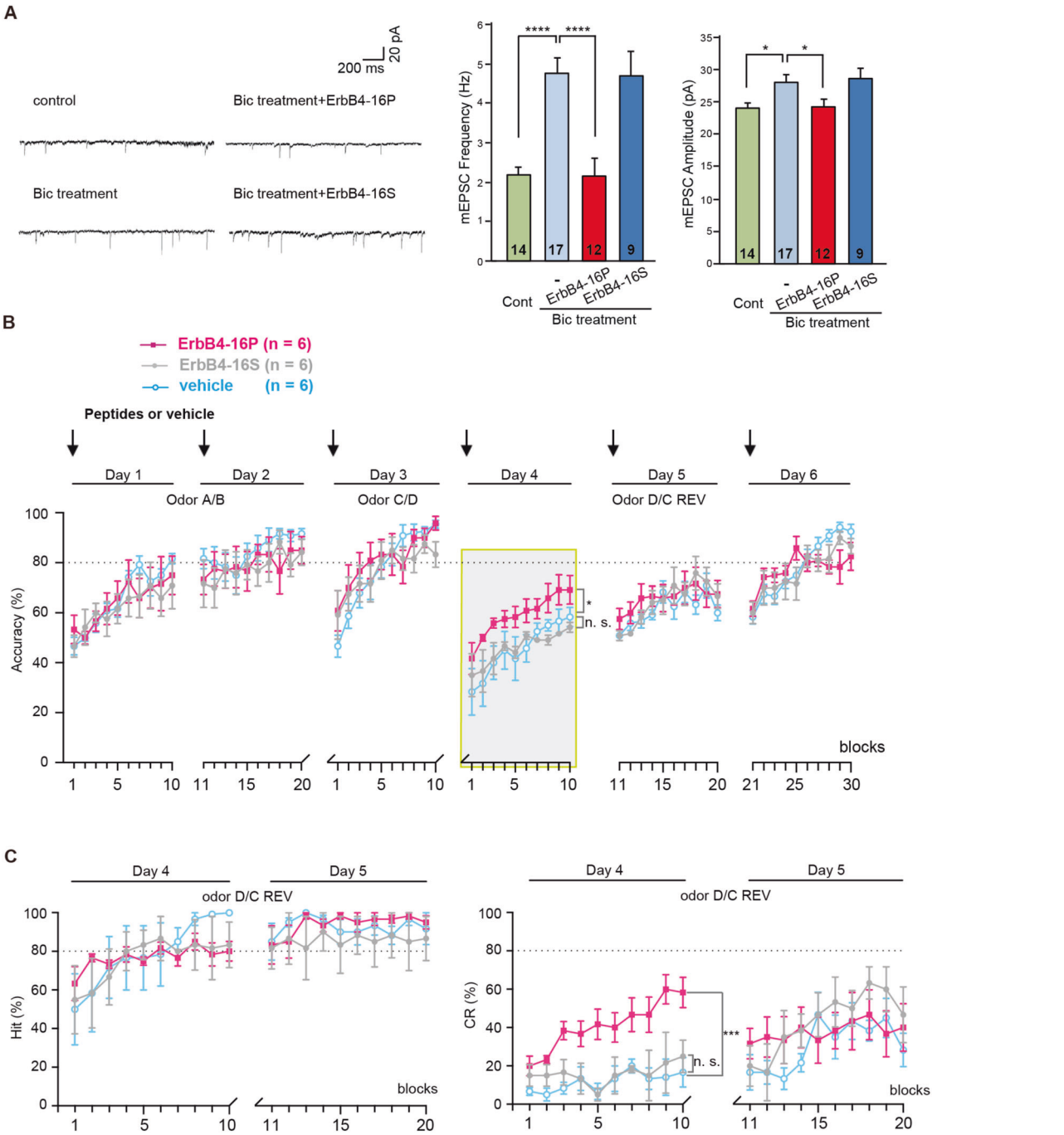

Fig. 5 Inhibition of ErbB4–NRXN1β interaction impairs excitatory synaptic plasticity of ErbB4-expressing interneurons and promotes olfactory associative reversal learning. A ErbB4-16P decreased mEPSC amplitude and frequency 24 h after bicuculline (Bic) treatment in cortical ErbB4^{+} neurons. ErbB4^{+} neurons were live-labeled using anti-extracellular ErbB4 fragment antibody. Representative traces of mEPSCs from four groups of primary cortical ErbB4^{+} interneurons in whole-cell configuration. Results are presented as mean ± SEM ($n = 14$, 17, 12, or 9 cells for each group shown in the figure, respectively, from three independent experiments). *$P < 0.05$, ****$P < 0.0001$. F(3, 48) = 13.31, Bic vs control (Cont), Bic + ErbB4-16P, Bic + ErbB4-16S: $P < 0.0001$, $P < 0.0001$, $P = 0.9990$ respectively for mEPSC Frequency. F(3, 48) = 4.131, Bic vs Cont, Bic + ErbB4-16P, Bic + ErbB4-16S: $P = 0.0344$, $P = 0.0471$, $P = 0.9874$ respectively for mEPSC Amplitude. One-way ANOVA with Dunnett's method. **B** Effect of intra-prelimbic cortex ErbB4-16P on olfactory associative learning. The tasks were performed after peptides (ErbB4-16P or ErbB4-16S) or vehicle administration for six days consecutively. Data shown are mean ± SEM ($n = 6$). *$P < 0.05$ (n.s. refers to non-significance). F (1, 10) = 0.005542, ErbB4-16S vs vehicle, $P = 0.9421$; F(1, 10) = 5.559, ErbB4-16P vs vehicle, $P = 0.0401$ in Day 4; two-way repeated-measures ANOVA. **C** Percentage of Hit or CR in Day 4 and Day 5. Data shown are mean ± SEM ($n = 6$). ***$P < 0.001$ (n.s. refers to non-significance). F(1, 10) = 0.3863, ErbB4-16S vs vehicle, $P = 0.5482$; F(1, 10) = 38.53, ErbB4-16P vs vehicle, $P = 0.0001$ in Day 4 of CR. F(1, 10) = 0.06, ErbB4-16S vs vehicle, $P = 0.8114$; F(1, 10) = 0.05526, ErbB4-16P vs vehicle, $P = 0.8199$ in Day 4 of Hit. Two-way repeated-measures ANOVA.

Overcoming proactive interference requires forgetting old conflicting information. The present work reveals a synaptic and molecular basis for PV interneurons mediating proactive interference, and suggests that NRXN1β-ErbB4 is a potential target for the treatment of susceptibility to proactive interference.

In summary, we provide evidence that ErbB4 is responsible for learning-induced excitatory synaptic transmission onto adult PV interneurons by directly binding presynaptic NRXN1β, which participates in proactive interference in learning. Our findings reveal a synaptic and molecular basis of local neuronal circuit remodeling for PV interneurons to sense corresponding network activity, providing a novel insight into cognitive processes. They may also contribute to a better understanding of attention and cognitive flexibility or their dysfunction.

REFERENCES

1. Crossley M, Lorenzetti FD, Naskar S, O'Shea M, Kemenes G, Benjamin PR, et al. Proactive and retroactive interference with associative memory consolidation in the snail Lymnaea is time and circuit dependent. Commun Biol. 2019;2:242.
2. Devkar DT, Wright AA. Event-based proactive interference in rhesus monkeys. Psychon Bull Rev. 2016;23:1474–82.
3. Wright AA, Katz JS, Ma WJ. How to be proactive about interference: lessons from animal memory. Psychol Sci. 2012;23:453–58.
4. Whissell PD, Cajanding JD, Fogel N, Kim JC. Comparative density of CCK- and PV-GABA cells within the cortex and hippocampus. Front Neuroanat. 2015;9:124.
5. Rudy B, Fishell G, Lee S, Hjerling-Leffler J. Three groups of interneurons account for nearly 100% of neocortical GABAergic neurons. Dev Neurobiol. 2011;71:45–61.
6. Hansen MG, Ledri LN, Kirik D, Kokaia M, Ledri M. Preserved function of afferent parvalbumin-positive perisomatic inhibitory synapses of dentate granule cells in rapidly kindled mice. Front Cell Neurosci. 2018;11:433.
7. Volman V, Behrens MM, Sejnowski TJ. Downregulation of parvalbumin at cortical GABA synapses reduces network gamma oscillatory activity. J Neurosci. 2011;31:18137–48.
8. Groisman AI, Yang SM, Schinder AF. Differential coupling of adult-born granule cells to parvalbumin and somatostatin interneurons. Cell Rep. 2020;30:202–14.
9. Tripodi M, Bhandari K, Chowdhury A, Mukherjee A, Caroni P. Parvalbumin interneuron plasticity for consolidation of reinforced learning. Cold Spring Harb Symp Quant Biol. 2018;83:25–35.
10. Favuzzi E, Marques-Smith A, Deogracias R, Winterflood CM, Sánchez-Aguilera A, Mantoan L, et al. Activity-dependent gating of parvalbumin interneuron function by the perineuronal net protein Brevican. Neuron 2017;95:639–55.
11. Ognjanovski N, Schaeffer S, Wu J, Mofakham S, Maruyama D, Zochowski M, et al. Parvalbumin-expressing interneurons coordinate hippocampal network dynamics required for memory consolidation. Nat Commun. 2017;8:15039.
12. Xia F, Richards BA, Tran MM, Josselyn SA, Takehara-Nishiuchi K, Frankland PW. Parvalbumin-positive interneurons mediate neocortical-hippocampal interactions that are necessary for memory consolidation. Elife 2017;6:e27868.
13. Alvarez DD, Giacomini D, Yang SM, Trinchero MF, Temprana SG, Büttner KA, et al. A disynaptic feedback network activated by experience promotes the integration of new granule cells. Science 2016;354:459–65.
14. Donato F, Rompani SB, Caroni P. Parvalbumin-expressing basket-cell network plasticity induced by experience regulates adult learning. Nature 2013;504:272–6.
15. Yin DM, Sun XD, Bean JC, Lin TW, Sathyamurthy A, Xiong WC, et al. Regulation of spine formation by ErbB4 in PV-positive interneurons. J Neurosci. 2013;33:19295–303.
16. Ting AK, Chen Y, Wen L, Yin DM, Shen C, Tao Y, et al. Neuregulin 1 promotes excitatory synapse development and function in GABAergic interneurons. J Neurosci. 2011;31:15–25.
17. Fazzari P, Paternain AV, Valiente M, Pla R, Luján R, Lloyd K, et al. Control of cortical GABA circuitry development by Nrg1 and ErbB4 signalling. Nature 2010;464:1376–80.
18. Vullhorst D, Neddens J, Karavanova I, Tricoire L, Petralia RS, McBain CJ, et al. Selective expression of ErbB4 in interneurons, but not pyramidal cells, of the rodent hippocampus. J Neurosci. 2009;29:12255–64.
19. Yau HJ, Wang HF, Lai C, Liu FC. Neural development of the neuregulin receptor ErbB4 in the cerebral cortex and the hippocampus: preferential expression by interneurons tangentially migrating from the ganglionic eminences. Cereb Cortex. 2003;13:252–64.
20. Huang YZ, Won S, Ali DW, Wang Q, Tanowitz M, Du QS, et al. Regulation of neuregulin signaling by PSD-95 interacting with ErbB4 at CNS synapses. Neuron 2000;26:443–55.
21. Deng W, Luo F, Li BM, Mei L. NRG1-ErbB4 signaling promotes functional recovery in a murine model of traumatic brain injury via regulation of GABA release. Exp Brain Res. 2019;237:3351–62.
22. Mei L, Nave KA. Neuregulin-ERBB signaling in the nervous system and neuropsychiatric diseases. Neuron 2014;83:27–49.
23. Mei L, Xiong WC. Neuregulin 1 in neural development, synaptic plasticity and schizophrenia. Nat Rev Neurosci. 2008;9:437–52.
24. Grieco SF, Wang G, Mahapatra A, Lai C, Holmes TC, Xu X. Neuregulin and ErbB expression is regulated by development and sensory experience in mouse visual cortex. J Comp Neurol. 2020;528:419–32.
25. Domínguez S, Rey CC, Therreau L, Fanton A, Massotte D, Verret L, et al. Maturation of PNN and ErbB4 signaling in area CA2 during adolescence underlies the emergence of PV interneuron plasticity and social memory. Cell Rep. 2019;29:1099–112.
26. Sun Y, Ikrar T, Davis MF, Gong N, Zheng X, Luo ZD, et al. Neuregulin-1/ErbB4 signaling regulates visual cortical plasticity. Neuron 2016;92:160–73.
27. Yang JM, Zhang J, Chen XJ, Geng HY, Ye M, Spitzer NC, et al. Development of GABA circuitry of fast-spiking basket interneurons in the medial prefrontal cortex of erbb4-mutant mice. J Neurosci. 2013;33:19724–33.
28. Chen YJ, Zhang M, Yin DM, Wen L, Ting A, Wang P, et al. ErbB4 in parvalbumin-positive interneurons is critical for neuregulin 1 regulation of long-term potentiation. Proc Natl Acad Sci USA. 2010;107:21818–23.
29. Corfas G, Roy K, Buxbaum JD. Neuregulin 1-erbB signaling and the molecular/cellular basis of schizophrenia. Nat Neurosci. 2004;7:575–80.
30. Barros CS, Calabrese B, Chamero P, Roberts AJ, Korzus E, Lloyd K, et al. Impaired maturation of dendritic spines without disorganization of cortical cell layers in mice lacking NRG1/ErbB signaling in the central nervous system. Proc Natl Acad Sci USA. 2009;106:4507–12.
31. Xu Y, Hou XY, Liu Y, Zong YY. Different protection of K252a and N-acetyl-L-cysteine against amyloid-beta peptide-induced cortical neuron apoptosis involving inhibition of MLK3-MKK7-JNK3 signal cascades. J Neurosci Res. 2009;87:918–27.
32. Janssen MJ, Leiva-Salcedo E, Buonanno A. Neuregulin directly decreases voltage-gated sodium current in hippocampal ErbB4-expressing interneurons. J Neurosci. 2012;32:13889–95.
33. Du CP, Wang M, Geng C, Hu B, Meng L, Xu Y, et al. Activity-induced SUMOylation of neuronal nitric oxide synthase is associated with plasticity of synaptic transmission and extracellular signal-regulated kinase 1/2 signaling. Antioxid Redox Signal. 2020;32:18–34.
34. Zhu QJ, Kong FS, Xu H, Wang Y, Du CP, Sun CC, et al. Tyrosine phosphorylation of GluK2 up-regulates kainate receptor-mediated responses and downstream signaling after brain ischemia. Proc Natl Acad Sci USA. 2014;111:13990–95.
35. Foggetti A, Baccini G, Arnold P, Schiffelholz T, Wulff P. Spiny and non-spiny parvalbumin-positive hippocampal interneurons show different plastic properties. Cell Rep. 2019;27:3725–32.
36. Kehagia AA, Murray GK, Robbins TW. Learning and cognitive flexibility: frontostriatal function and monoaminergic modulation. Curr Opin Neurobiol. 2010;20:199–204.
37. Takehara-Nishiuchi K, McNaughton BL. Spontaneous changes of neocortical code for associative memory during consolidation. Science 2008;322:960–3.
38. Anderson GR, Aoto J, Tabuchi K, Földy C, Covy J, Yee AX, et al. β-Neurexins control neural circuits by regulating synaptic endocannabinoid signaling. Cell 2015;162:593–606.
39. Futai K, Doty CD, Baek B, Ryu J, Sheng M. Specific trans-synaptic interaction with inhibitory interneuronal neurexin underlies differential ability of neuroligins to induce functional inhibitory synapses. J Neurosci. 2013;33:3612–23.
40. Shipman SL, Nicoll RA. Dimerization of postsynaptic neuroligin drives synaptic assembly via transsynaptic clustering of neurexin. Proc Natl Acad Sci USA. 2012;109:19432–7.
41. Donato F, Chowdhury A, Lahr M, Caroni P. Early- and late-born parvalbumin basket cell subpopulations exhibiting distinct regulation and roles in learning. Neuron 2015;85:770–86.
42. Südhof TC. Neuroligins and neurexins link synaptic function to cognitive disease. Nature 2008;455:903–11.
43. Ma L, Huang YZ, Pitcher GM, Valtschanoff JG, Ma YH, Feng LY, et al. Ligand-dependent recruitment of the ErbB4 signaling complex into neuronal lipid rafts. J Neurosci. 2003;23:3164–75.
44. Meng L, Du CP, Lu CY, Zhang K, Li L, Yan JZ, et al. Neuronal activity-induced SUMOylation of Akt1 by PIAS3 is required for long-term potentiation of synaptic transmission. FASEB J. 2021;35:e21769.
45. Yang JM, Shen CJ, Chen XJ, Kong Y, Liu YS, Li XW, et al. erbb4 deficits in chandelier cells of the medial prefrontal cortex confer cognitive dysfunctions: implications for schizophrenia. Cereb Cortex. 2019;29:4334–46.

46. Epp JR, Silva Mera R, Köhler S, Josselyn SA, Frankland PW. Neurogenesis-mediated forgetting minimizes proactive interference. Nat Commun. 2016;7:10838.
47. Madan CR, Fujiwara E, Gerson BC, Caplan JB. High reward makes items easier to remember, but harder to bind to a new temporal context. Front Integr Neurosci. 2012;6:61.
48. Jung MW, Baeg EH, Kim MJ, Kim YB, Kim JJ. Plasticity and memory in the prefrontal cortex. Rev Neurosci. 2008;19:29–46.
49. Jeong H, Kim D, Song M, Paik SB, Jung MW. Distinct roles of parvalbumin- and somatostatin-expressing neurons in flexible representation of task variables in the prefrontal cortex. Prog Neurobiol. 2020;187:101773.
50. Guise KG, Shapiro ML. Medial prefrontal cortex reduces memory interference by modifying hippocampal encoding. Neuron 2017;94:183–92.
51. Whitmire CJ, Stanley GB. Rapid sensory adaptation redux: a circuit perspective. Neuron 2016;92:298–315.
52. Winstanley CA, Floresco SB. Deciphering decision making: variation in animal models of effort- and uncertainty-based choice reveals distinct neural circuitries underlying core cognitive processes. J Neurosci. 2016;36:12069–79.
53. Chen LY, Jiang M, Zhang B, Gokce O, Südhof TC. Conditional deletion of all neurexins defines diversity of essential synaptic organizer functions for neurexins. Neuron 2017;94:611–25.
54. Li MY, Miao WY, Wu QZ, He SJ, Yan G, Yang Y, et al. A critical role of presynaptic Cadherin/Catenin/p140Cap complexes in stabilizing spines and functional synapses in the neocortex. Neuron 2017;94:1155–72.
55. Sytnyk V, Leshchyns'ka I, Schachner M. Neural cell adhesion molecules of the immunoglobulin superfamily regulate synapse formation, maintenance, and function. Trends Neurosci. 2017;40:295–308.
56. Dean C, Scholl FG, Choih J, DeMaria S, Berger J, Isacoff E, et al. Neurexin mediates the assembly of presynaptic terminals. Nat Neurosci. 2003;6:708–16.
57. Sugita S, Saito F, Tang J, Satz J, Campbell K, Südhof TC. A stoichiometric complex of neurexins and dystroglycan in brain. J Cell Biol. 2001;154:435–45.
58. Südhof TC. Synaptic neurexin complexes: a molucular code for the logic of neural circuits. Cell 2017;171:745–69.
59. Ibata K, Kono M, Narumi S, Motohashi J, Kakegawa W, Kohda K, et al. Activity-dependent secretion of synaptic organizer Cbln1 from lysosomes in granule cell axons. Neuron 2019;102:1184–98.
60. Peixoto RT, Kunz PA, Kwon H, Mabb AM, Sabatini BL, Philpot BD, et al. Transsynaptic signaling by activity-dependent cleavage of neuroligin-1. Neuron 2012;76:396–409.
61. Meis S, Endres T, Munsch T, Lessmann V. Impact of chronic BDNF depletion on GABAergic synaptic transmission in the lateral amygdala. Int J Mol Sci. 2019;20:4310.
62. Duman RS, Deyama S, Fogaça MV. Role of BDNF in the pathophysiology and treatment of depression: activity-dependent effects distinguish rapid-acting antidepressants. Eur J Neurosci. 2021;53:126–39.
63. Czéh B, Vardya I, Varga Z, Febbraro F, Csabai D, Martis LS, et al. Long-term stress disrupts the structural and functional integrity of GABAergic neuronal networks in the medial prefrontal cortex of rats. Front Cell Neurosci. 2018;12:148.
64. Samrani G, Bäckman L, Persson J. Age-differences in the temporal properties of proactive interference in working memory. Psychol Aging. 2017;32:722–31.
65. Smets J, Wessel I, Raes F. Reduced autobiographical memory specificity relates to weak resistance to proactive interference. J Behav Ther Exp Psychiatry. 2014;45:234–41.
66. Daneshvar S, Taghavi MR, Goodarzi MA, Jobson L. Emotionally valenced and modality-specific dual tasks: effects on voluntary reminding and proactive interference in trauma-exposed individuals suffering from PTSD. Psychol Trauma. 2021;13:586–95.

ACKNOWLEDGEMENTS

We would like to thank Prof. Lin Mei at Case Western Reserve University and Prof. Yanmei Tao at Hangzhou Normal University for helpful discussions on experimental design. We also thank Prof. Lin Mei for kindly providing PV-Cre mice, floxed *Erbb4* mice, and NRXN1βNTF plasmids.

AUTHOR CONTRIBUTIONS

Design of experiments: YX and XYH. Investigation and data acquisition: YX, MLW, HT, CG, FG, BH, RW. Data analysis: YX, MLW, CG, and BH. Writing-original draft: YX. Conception, revision of manuscript, and funding: XYH. All authors approved the final manuscript before submission.

FUNDING

This work was supported by grants from the National Natural Science Foundation of China (81673418 and 81473185) and a project founded by the Jiangsu 333 program (BRA2018059).

COMPETING INTERESTS

The authors declare no competing interests.

ADDITIONAL INFORMATION

Supplementary information The online version contains supplementary material available at https://doi.org/10.1038/s41386-021-01205-0.

Correspondence and requests for materials should be addressed to Xiao-Yu Hou.

Reprints and permission information is available at http://www.nature.com/reprints

Publisher's note Springer Nature remains neutral with regard to jurisdictional claims in published maps and institutional affiliations.